NASA
Technical
Paper
2562

February 1986

Passive Eddy-Current Damping as a Means of Vibration Control in Cryogenic Turbomachinery

Robert E. Cunningham

NASA

NASA Technical Paper 2562

1986

Passive Eddy-Current Damping as a Means of Vibration Control in Cryogenic Turbomachinery

Robert E. Cunningham

Lewis Research Center
Cleveland, Ohio

National Aeronautics and Space Administration

Scientific and Technical Information Branch

Summary

Experiments were conducted with a rotating test apparatus to evaluate eddy-current damping as a means of reducing lateral shaft vibrations.

A vertically oriented rotor was operated over a speed range from 800 to 10 000 rpm. A damper assembly comprising four permanent magnets and four copper conductors was located at the lower ball-bearing support, and was completely immersed in liquid nitrogen during the test runs.

Lateral shaft vibrations were induced by an unbalance (10.8 g cm) located in a 15.2-cm-diameter steel disk attached to the rotor.

Three permanent magnet/conductor combinations were tested in liquid nitrogen to determine the magnitude of damping and to compare the results with values of damping coefficients calculated from magnet/conductor characteristics at a temperature of −197 °C.

The original, or baseline, damper assembly consisted of four equally spaced, C-shaped, Alnico 5 magnets and four high-purity copper conductors. The experimentally determined damping coefficients in liquid nitrogen at −197 °C were 530 and 240 N sec/m, as measured along coordinate axes. The theoretical damping coefficients, as calculated for four symmetrically arranged magnet/conductors, were 650 N sec/m along the *X*-axis and 270 N sec/m along the *Y*-axis.

A second design consisted of the same C-shaped, Alnico 5 magnets modified to create a narrower gap, and thus a greater flux density, by the addition of a steel pole piece. The experimentally determined damping coefficients were 180 and 400 N sec/m as calculated by the one-half power-point method at the resonant frequency. The theoretical coefficients were 370 and 150 N sec/m along the *X*- and *Y*-axes, respectively. Although the gap flux density increased by 30 percent, the measured damping was not increased proportionally. The decreased volume of conductor material available in the narrower gap negated the increased flux effect.

A third damper assembly also used Alnico 5 magnets, however, with rare-earth, rectangular-magnet pole faces. The experimentally determined damping coefficients were 500 and 320 N sec/m along the *X*- and *Y*-axes, respectively. The theoretical damping coefficients were calculated to be 780 N sec/m along the *X*-axis and 330 N sec/m along the *Y*-axis. Experimental damping coefficients were lower than those calculated from magnet and conductor properties, but the agreement is reasonable.

Although for the designs tested experimental damping coefficients were not large in magnitude, they do demonstrate that eddy-current damping is a viable means to control vibration in cryogenic turbomachinery. Increased damping is possible with designs that incorporate a greater number of magnets, and/or the use of higher energy rare-earth magnet materials such as samarium-cobalt ($Sm\text{-}Co_5$) and neodymium-iron-boron (Nd-Fe-B).

Experimentally obtained, rotor-response plots were compared with those generated by a modified unbalance-response computer code. The agreement was reasonably good for the theoretical damping values of 100 and 430 N sec/m. The unbalance magnitude and spring rate that were used in the theoretical program input were identical to those used in the experimental apparatus.

Introduction

The need for dissipating vibrational energy in high-performance turbomachines has been recognized for a long time. Many of today's turbojet engines, in both commercial and military aviation, employ vibration dampers at, or near, bearing supports. Because of the ready availability of lubricating oils in aircraft engines, a device known as a squeeze film damper is regularly used to suppress large and potentially damaging whirl forces (ref. 1).

In the space shuttle main engine (SSME) turbopumps, liquid hydrogen and liquid oxygen cool the rolling-element bearings. Because of the low viscosity of these liquids (liquid hydrogen has a viscosity approximately equal to air at room temperature), they cannot be considered adequate for viscous damping.

Cryogenic turbomachinery of the type used to pump high-pressure fuel (liquid hydrogen at −253 °C) and oxidizer (liquid oxygen at −183 °C) to the main engines of the space shuttle can be subjected to lateral rotor vibrations from unbalance forces. Bearing failures early in the development of these turbopumps limited the magnitude of the power level to which the space shuttle main engines could be operated (ref. 2).

Hysteresis in the internal shaft and friction between the relatively moving surfaces in the rotor assembly and the labyrinth seals were two of many sources of excitation for subsynchronous whirl (ref. 3). This type of instability can be particularly damaging because the amplitude of the whirl orbit

increases rapidly with increasing energy input. Both kinds of whirling can generate excessive bearing loads that significantly reduce bearing life.

Current turbopump designs do not include provisions for final trim balancing of the built-up rotor after final assembly in the pump casing. Individual component balancing does not always ensure a satisfactorily balanced assembly (ref. 2). The need to attenuate vibration is obvious; the means chosen, however, must be compatible with the severe temperature environment.

Hysteresis damping, the type produced by the cyclic deformation of viscoelastic materials such as rubber, is a common method of damping over a modest temperature range. However, these materials would not retain their viscoelastic properties at cryogenic temperatures.

Coulomb or friction damping is another energy dissipation concept having limited application in turbomachinery. The force in such a damper is proportional to the applied pressure between the two relatively moving surfaces. The constant of proportionality is the coefficient of friction between the two surfaces, and is, in most cases, difficult to quantify.

Eddy-current damping, the focus of this research effort, is another mechanism for vibration attenuation. Eddy currents are induced in a nonferrous conductor that is vibrating in a plane normal to the magnetic flux field generated by a permanent magnet. Eddy-current damping is similar to oil-viscous damping in that the damping force is directly proportional to velocity. The constant of proportionality is known as the damping coefficient and is a function of the magnetic flux, conductor volume, and conductor-material resistivity (ref. 4).

The low-temperature environment of the SSME turbopumps that renders most conventional forms of damping ineffectual actually enhances eddy-current damping. Flux density at liquid-oxygen temperatures is slightly increased (approx. 0.05-percent/°C). Resistivity decreases by almost a factor of 10 for high-purity copper. At liquid-hydrogen temperatures, the resistivity decreases by another factor of 10, that is, one one-hundredth of the resistivity at room temperature. Because the damping coefficient is inversely proportional to the resistivity, its value increases as the resistivity decreases.

The experimental research effort reported here was limited to results obtained with eddy-current dampers composed of permanent magnets. Electromagnets would produce similar results, but, perhaps, with additional complexity. Efforts along this line are recommended for future study.

The damper designs tested were also limited to magnet materials readily available from domestic vendors: materials such as Alnico 5 (8 Al, 14 Ni, 24 Co, 3 Cu, bal Fe) and rare-earth materials such as samarium-cobalt.

A rotating test apparatus was used to provide steady-state rotor vibrations that could be measured, and thus permitted the calculation of appropriate eddy-current damping and stiffness coefficients. Results were obtained for three basic damper designs over a speed range from approximately 800 to 10 000 rpm while the damper was totally immersed in liquid nitrogen. An unbalance of 10.8 g cm was used to provide the steady-state excitation.

The objectives of this study of damper designs were as follows:

(1) To establish baseline damping data for a simple C-shaped configuration of Alnico 5 magnet material

(2) To decrease the length of the pole face gap of the C-shaped magnet and thus increase its flux density, and determine if the increased flux density would result in greater damping

(3) To determine whether the increased coercive force of rare-earth pole pieces could provide greater damping (The third design would again be a C-shaped magnet but two rare-earth rectangular magnets would be added to it as pole faces.)

Apparatus

Mechanical Features

Experimental results were obtained with the apparatus depicted in figures 1 and 2. The apparatus consists of a slender shaft, 50.8 cm in length. It is supported vertically in two rolling-element bearings located approximately 44.6 cm apart.

A disk of 15.2-cm diameter is attached to the shaft to provide additional inertia to the rotating system and to serve as a means of adding a known amount of unbalance (in the form of small set screws located at a 6.4-cm radius in the disk). This assembly with the bearings installed was balanced in a two-plane dynamic balancer to less than 0.0025-mm peak-to-peak runout.

The outer race of the lower, 20-mm bore, angular-contact bearing is located in a thin-walled cylinder commonly referred to as a squirrel cage spring. The average stiffness of this spring measured along the two axes was 2.54×10^6 N/m.

The shaft is driven by a 2.2-kW (3-hp), frequency-controlled, ac motor through a timing-belt pulley arrangement. The test shaft operates at twice the speed of the motor shaft with an upper limit of approximately 12 000 rpm.

A steel, vacuum-jacketed vessel bolts onto the rig support structure and completely encloses the lower bearing-damper assembly. When the inner chamber is filled with liquid nitrogen the bearing and damper assembly are completely immersed. Each of the four C-shaped, permanent magnets in the damper assembly are attached to the free end of a cantilevered beam. Each beam is bolted to a movable plate capable of 45° of rotation about the shaft centerline. This arrangement permits the four magnets to be rotated relative to the individual copper conductors attached to the squirrel cage spring. The conductors were made of oxygen-free copper, 99.99-percent chemically pure.

For the tests conducted in this investigation the relationship of conductor to pole face remained the same, that is, the four conductor segments were aligned centrally between the magnet pole faces, as shown in the damper-assembly plan view of figure 3. Also shown in this figure are the relative positions

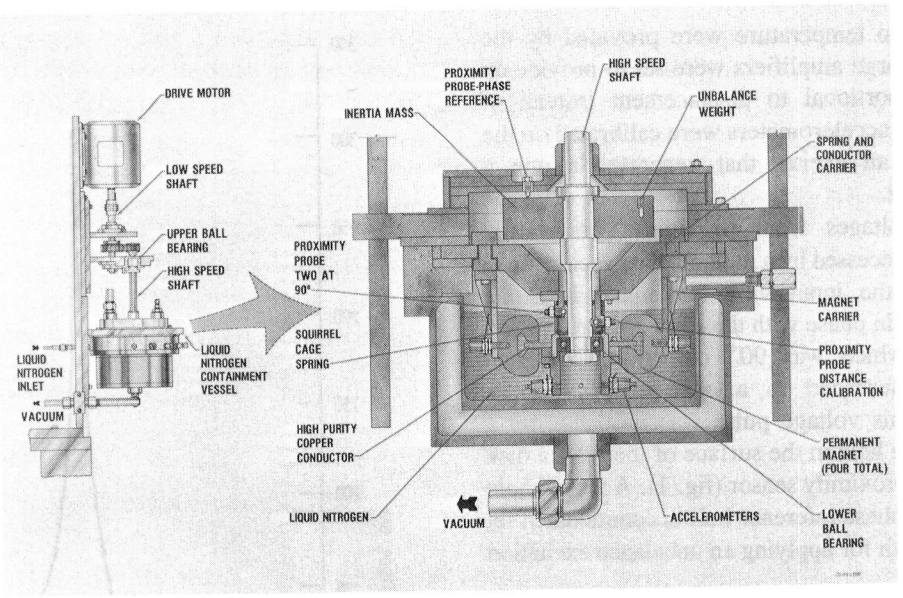

Figure 1.—Eddy-current damper test apparatus.

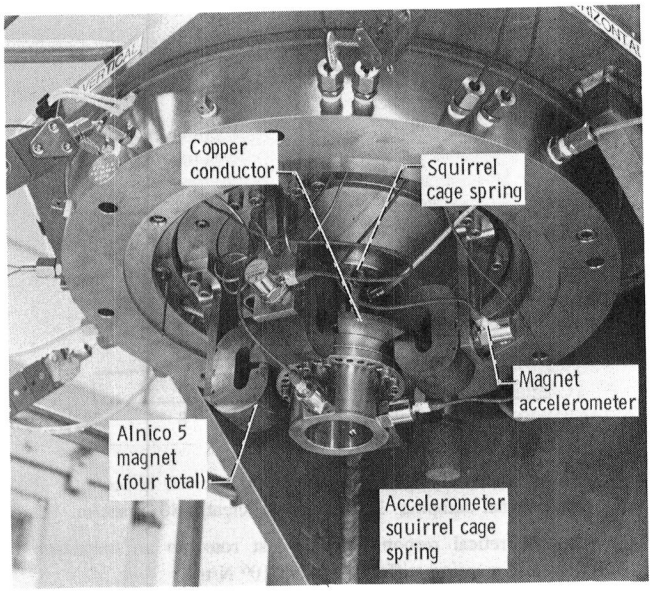

Figure 2.—Photograph of eddy-current damper assembly.

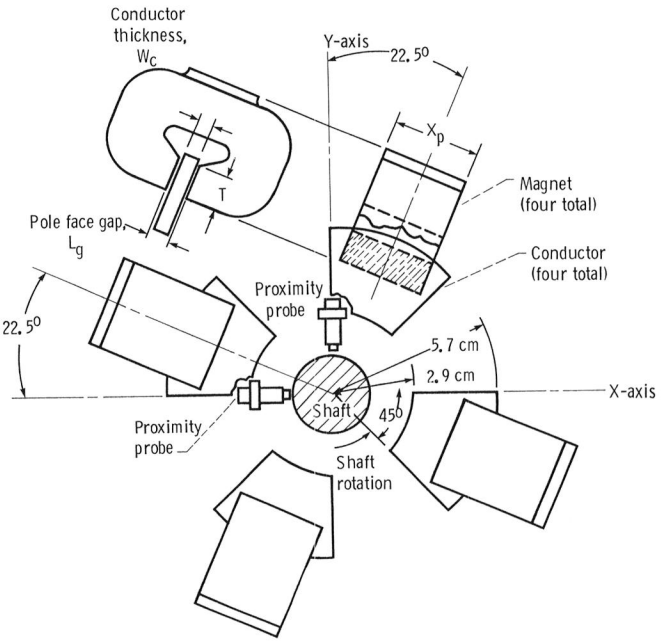

Figure 3.—Plan view of the damper assembly and location of the proximity probes.

of the magnet/conductor axes to the proximity-probe axes. The magnet axes are 22.5° from the proximity-probe axes.

Instrumentation

Lateral deflections of the test rotor from a neutral axis were sensed by eddy-current proximity probes (figs. 1 and 3). These probes, along with their signal conditioners and power supply, produce a voltage that is linearly proportional to distance. The approximate linear range for these probes was 0.72 to 1.02 mm. These proximity probes were calibrated at room temperature with the same material used to make the shaft—stainless steel. A third probe, identical to the other two, was located opposite a notch milled into the rotor surface, but below the plane where the other two probes were located. The notch served to detect the change in probe sensitivity when the ambient temperature was lowered to −197 °C.

Two accelerometers attached to the ball-bearing support spring were used to monitor vibratory response caused by the shaft unbalance. An additional two accelerometers that were mounted on two of the magnet support arms were used to monitor the motion transmitted through the magnets to the support structure; these accelerometers are shown in figure 1.

Accelerometer calibration factors supplied by the manufacturer were set into each charge amplifier. Variation

of these factors due to temperature were provided by the manufacturer. The charge amplifiers were set to provide an output that was proportional to displacement instead of acceleration. Then the accelerometers were calibrated on the test apparatus using an exciter that generated a one g acceleration at 100 Hz.

Cyclic, varying voltages from proximity probes and accelerometers were processed by a multichannel vector filter. The filter separated the input vibration signal into one component which was in phase with the rotor frequency, and another component which was 90° out of phase. Both components were referenced to a once-per-cycle pulse (Keyphase signal). This voltage pulse was produced by a drilled phase-reference hole in the surface of the inertia disk as it passed beneath a proximity sensor (fig. 1). A tapped hole located 180° from the phase reference hole accommodated set screws of varying length for applying an unbalance excitation to the rotor.

Each channel of the filter provided band-pass filtering of signals relative to the phase reference signal. The cyclic, varying signals were converted to proportional dc-voltage levels which were supplied as output signals to an externally connected data-acquisition system.

A modular instrument computer (MINC) was used to convert analog voltage signals to digital format for use in data processing. Digital values of voltage representing vibration amplitudes, phase angles, and rotor speeds were processed, plotted, and displayed in appropriate format on the computer screen. Amplitude-phase data from each test were stored on a flexible disk. A thermal printer was used to obtain hard copies of both the tabulated and plotted data.

Copper-constantan thermocouples were installed at the lower ball bearing and in two of the four copper conductors. Thermocouples were also used in the liquid-nitrogen containment vessel as a means of sensing high and low liquid levels. This was a permissive system which would shut down the drive motor in the event of too low a nitrogen level. In the event of too high a nitrogen level, it would shut down the supply of liquid nitrogen from the dewar.

The primary method of liquid level control was based on a principle of detecting the difference in the heat-transfer rate at the surface of a self-heating element between the liquid and vapor phases of the liquid nitrogen. The level sensing device operated a solenoid valve in the liquid-nitrogen supply line.

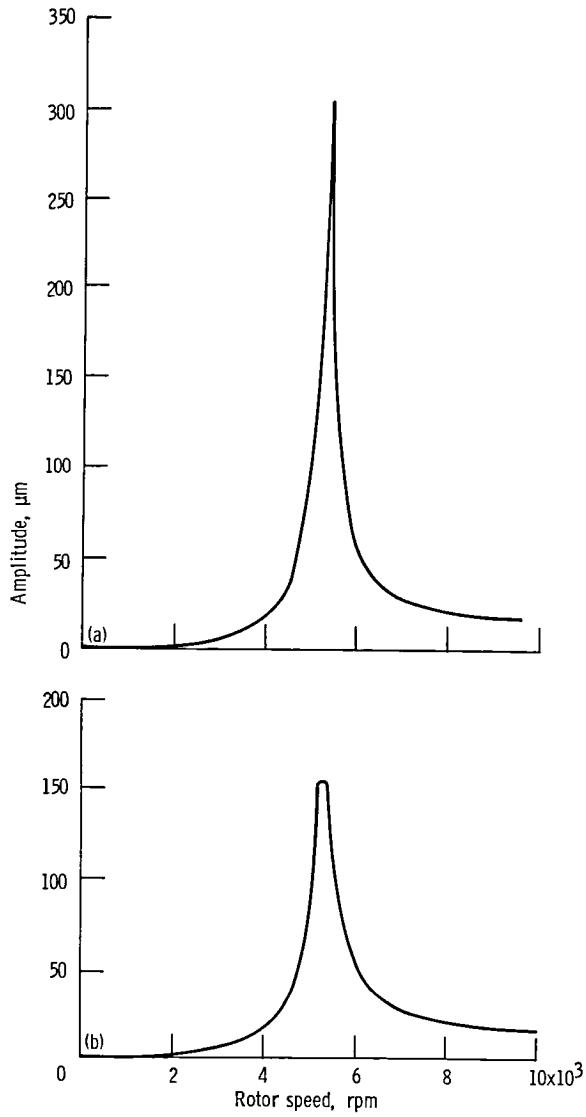

(a) Internal damping. Damping coefficient, 109 N sec/m.
(b) External damping. Damping coefficient, 440 N sec/m.

Figure 4.—Theoretical response of the test rotor to an unbalance of 10.8 g cm and a spring stiffness of 1.95 10^6 N/m.

Damper Design and Analysis

The overall size and number of magnets which comprise the experimental damper assembly was determined by the magnitude of the damping required to reduce the shaft excursion at the synchronous resonant frequency to approximately one-half that for an essentially undamped rotor (fig. 4). The three magnet designs tested are shown in figure 5 along with their dimensions, materials, and pole-face-gap flux densities.

A cast C-shape was chosen because it could provide a suitable, narrow pole face gap for the conductor, as well as an uninterrupted magnetic path. The lines of magnetic flux were then oriented normal to the conductor. A magnet assembly of short, straight magnets could have been used to achieve a C-shape; however, the joint reluctance encountered at each interface would have significantly reduced the flux density across the gap (ref. 5). The C-shaped magnets are made of a magnet material known as Alnico 5, an aluminum-nickel-cobalt-copper-iron alloy. This fairly common magnet material is readily available from most magnet vendors. Alnico 5 has a reasonably high energy product of 44 to 46.8 MJ/m³ (5.5

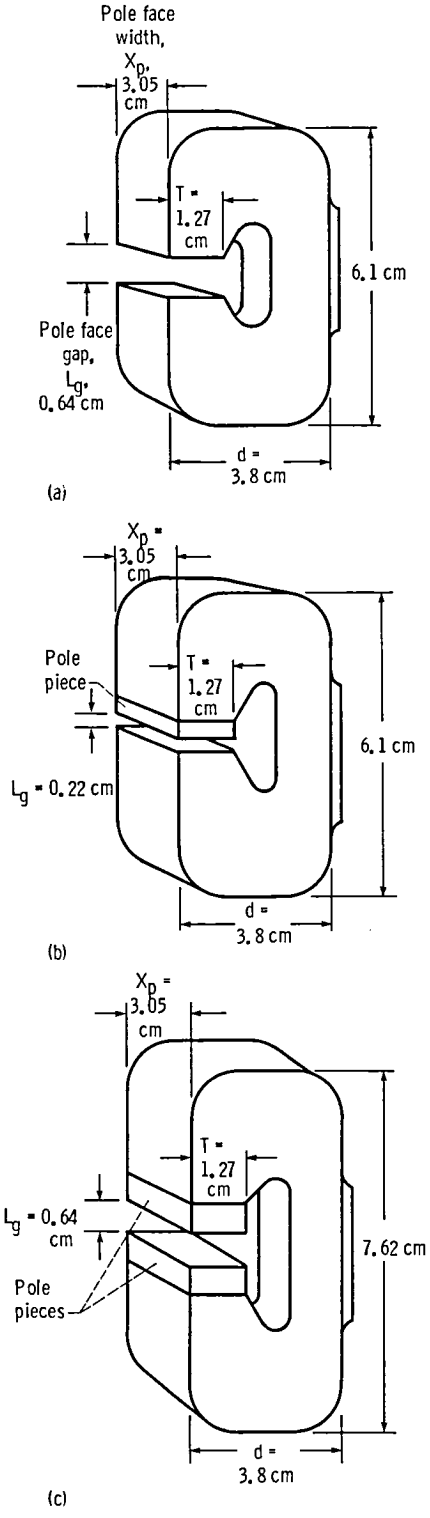

(a) Design A; pole face material, Alnico 5; pole face gap, L_g, 0.64 cm. Maximum measured flux density in gap, 0.54 T.

(b) Design B; pole face material low-carbon steel; pole face gap, L_g, 0.22 cm. Maximum measured flux density in gap, 0.7 T.

(c) Design C; pole face material, samarium-cobalt; pole face gap, L_g, 0.64 cm. Maximum measured flux density in gap, 0.59 T.

Figure 5.—Permanent magnet designs for evaluation in liquid nitrogen. Magnet material, Alnico 5; air temperature in gap, 22 °C. These dimensions were the same for all the designs: T, X_p, d.

to 5.8 MG Oe) and is capable of being cast into the desired C-shape.

For all three designs the flux density across the pole face gap was determined from the empirical design formulas and hysteresis curves for Alnico 5 as given in reference 6. Actual values of the flux density in the pole face gap were measured with a Hall-effect meter for each magnet in the assembly before its installation in the rig. Agreement between the calculated and measured magnetic-flux density was not, for the most part, good. For design A the calculated value for the maximum flux density in the pole face gap was 0.47 T, and the measured value was 0.54 T. For design C the calculated value was 0.83 T and the measured value was 0.59 T—a significant difference. (A calculated value for design B was not obtained because of insufficient magnetic data on the low-carbon-steel pole face used. The measured maximum flux density was 0.7 T.) The disagreement between the calculated and measured values of pole-face-gap flux densities was probably due to the following factors:

(1) The Alnico 5 magnet was demagnetized when in proximity to the high-coercive-force samarium-cobalt ($Sm\text{-}Co_5$) pole faces. Alnico 5 has a coercive force of only 52.8 kAm (660 Oe) compared with 664 kAm (8300 Oe) for $Sm\text{-}Co_5$.

(2) In addition, the magnetic reluctance at the magnet-pole interface decreased the effective flux density in the pole face gap. It was originally thought that the remanence flux of the individual magnet materials would be additive, and that the Alnico 5 magnet with the $Sm\text{-}Co_5$ pole faces would produce a total remanence flux for the combined assembly that was approximately equal to the sum of the individual magnets; however, this did not occur.

It is possible that initially combining the two magnet materials in the unmagnetized state and then magnetizing the assembly to the force required for the higher coercive material ($Sm\text{-}Co_5$) might achieve the desired results.

An expression for a damping coefficient can be derived from some basic laws of magnetism. Faraday's and Lenz's laws of magnetic induction can be stated in equation forms that relate to nonferrous, conducting material moving perpendicularly to a magnetic-flux field (fig. 6). One such derivation is given in reference 5. The conductor geometry in this expression is relatively small in cross-sectional area compared with its length.

However, another expression developed in reference 7 more closely resembles the geometry of the conductors used in these tests, that of a flat plate having considerable volume between the magnet pole faces (fig. 6). The actual expression derived in reference 7 is for a braking force acting on an infinitely long strip; this is analogous to a damping force since it opposes the motion. An expression for the damping coefficient C_D, can be obtained from this expression by remembering that the damping force is linearly proportional to velocity and the damping coefficient is the constant of proportionality. The resulting equation for the damping coefficient is

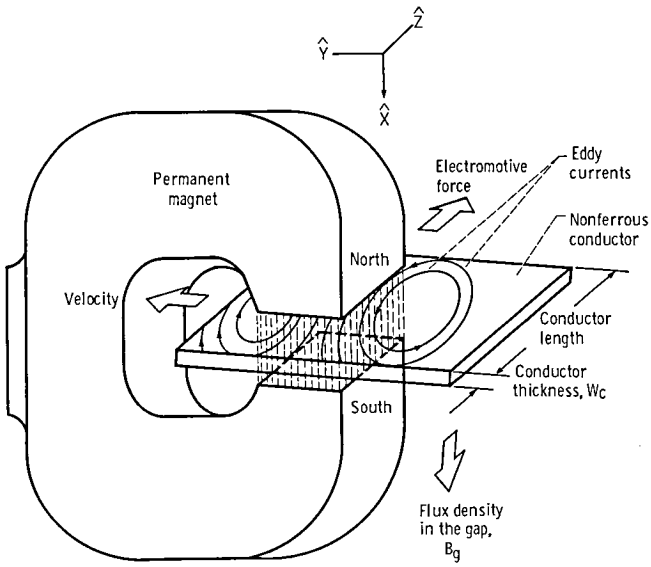

Figure 6.—Schematic of an eddy-current damper which shows the induced eddy-current paths in the conductor.

$$C_D = \frac{B_g^2 X_p^2 W_c L_i}{\rho \mu_0} \text{ N sec/m}$$

where

B_g flux density in gap, Wb/m^2
L_i inductivity per unit length
W_c conductor thickness, m
X_p pole face width, m
μ_0 permeability
ρ conductor resistivity, Ω m

The above expression was used to calculate the theoretical damping coefficients for the three designs (table I). The value of ρ was that for high-purity copper at 76 K (−197 °C) (fig. 7). The remanence flux density B_r for Alnico 5 at −197 °C was higher than the remanence flux density at room temperature. This increased value was based upon the empirical data (fig. 8).

Procedure

The rotor for the test apparatus, with its inertia disk installed, was balanced in a dynamic balancer. After assembly in the rig and before damped tests were run, the rotor was operated over the speed range 800 to 10 000 rpm to determine its state of balance. A runout no greater than 0.005 mm was observed. It was decided that this was a satisfactory balance for the tests contemplated.

The tare damping for the rotating system was established before installing any magnets in the apparatus. For an unbalance of 10.8 g cm, the system tare damping was observed

TABLE I.—SUMMARY OF EXPERIMENTAL AND THEORETICAL EDDY-CURRENT DAMPING COEFFICIENTS IN LIQUID NITROGEN

[Test conditions: Rotor speed 800 to 10 000 rpm; unbalance, 10.8 g cm; spring stiffness, 2.54×10^6 N/m.]

(a) Damped system response

Design (a)	Axis	Damping coefficient, N sec/m	
		Experimental[b]	Theoretical
A	X	530	650
	Y	240	270
B	X	400	370
	Y	180	150
C	X	500	780
	Y	320	330

(b) Undamped system response

Axis	Maximum peak-to-peak amplitude, μm	Resonant frequency, rpm	Tare damping coefficient, N sec/m
X	691	6100	70
Y	617	6100	110

[a]See fig. 5.
[b]Tare damping has been subtracted.

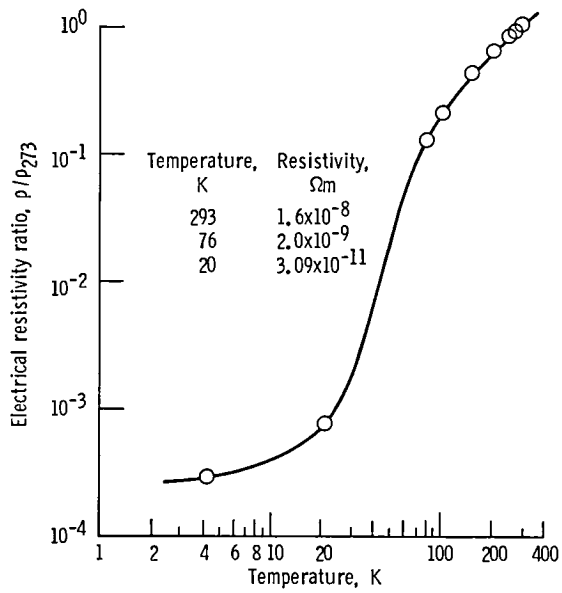

Figure 7.—Electrical resistivity of high-purity, oxygen-free copper as function of temperature. Electrical resistivity at 273 °C, ρ_{273}, 1.545×10^{-8} Ω m. (Data from ref. 9.)

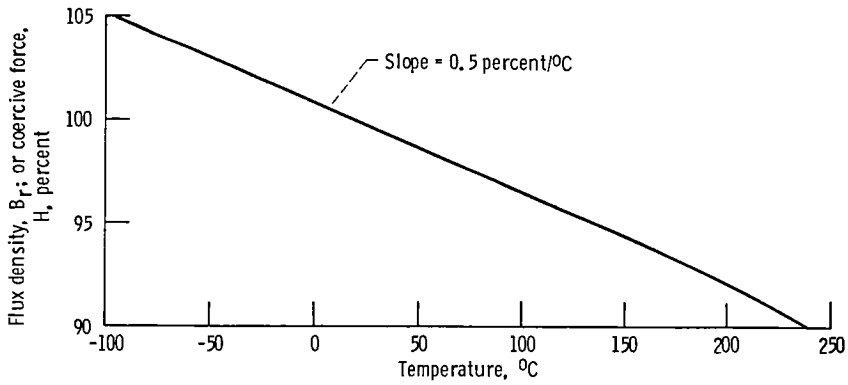

Figure 8.—Reversible temperature changes in remanence flux and coercivity at the operating point. Magnet material, Alnico 5. (Manufacturer's data.)

to be 70 N sec/m along the *X*-axis and 110 N sec/m along the *Y*-axis.

Before installing the magnets in the test apparatus, several readings were made of the flux density in the air gaps of the four magnets. This was done using a Bell model 630 gaussmeter. Flux densities were measured again after the magnets were installed in the apparatus. Generally, no significant change could be observed in the readings due to the proximity of the one magnet to the other.

Upon installation each copper conductor was inspected to ensure that adequate clearance existed on either side, between the conductor and the magnet pole face. The total clearance between the conductor and the pole-face gap was nominally 1.3 mm.

A specific procedure was followed before each test. All instrumentation was turned on to allow a warm up. A nitrogen gas purge was made of the containment vessel. A check was made of the two proximity probes at room temperature. The voltage was noted when a 0.025-cm slot in the shaft was rotated under one of the proximity probes. Nitrogen gas from a pressurized bottle was supplied to the 160-liter nitrogen dewar and regulated. A solenoid-operated nitrogen fill valve was actuated to allow liquid nitrogen to flow into the containment vessel.

After an approximately 10- to 15-min cool down, the proximity probes were rechecked by rotating the shaft and observing the voltage change when the 0.025-cm slot passed under the proximity probe. The calibration factor determined in this manner was then typed into the computer along with other data to identify the test run.

After about 20 min of soaking in liquid nitrogen, the temperatures of the conductors and the lower bearing had reached −192 °C. At this time power to the drive motor was turned on, and the computer was set to begin recording data. The ac motor drive was turned on. (It would come up to 800 rpm, the minimum shaft speed that could be set.) The rotor was slowly accelerated manually through the speed range while the computer accessed and processed the data. After reaching the maximum speed that was preset into the computer, the motor was allowed to decelerate to the minimum speed. Printouts were obtained for the rotor amplitude and phase angle versus frequency in tabular and plotted form. All accessed data were stored on flexible disk.

Results and Discussion

The results of this investigation are presented in figures 9 to 14 and also in table I. Three magnet designs were tested, details of which are given in figure 5. For all tests the synchronous response of the rotor to a preset unbalance of 10.8 g cm was recorded and plotted by computer. A peak-to-

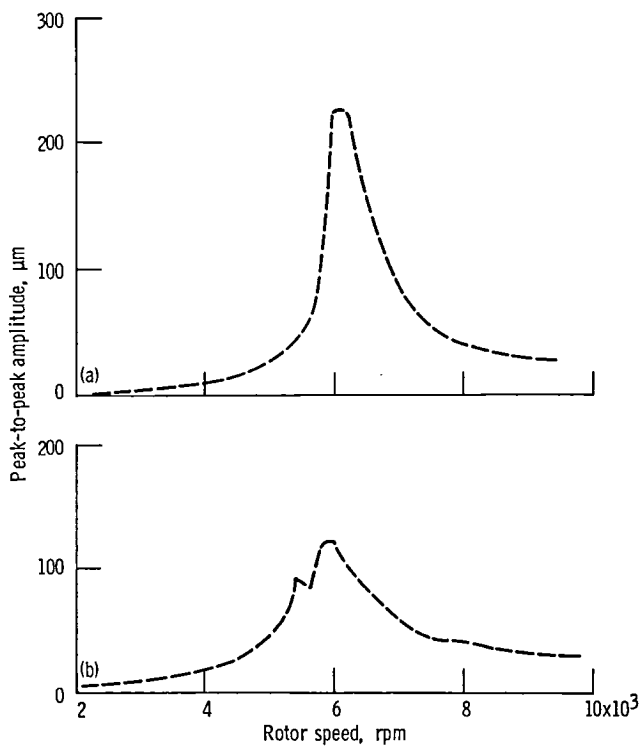

(a) *Y*-axis. Damping coefficient, C_D, 350 N sec/m.
(b) *X*-axis. Damping coefficient, C_D, 600 N sec/m.

Figure 9.—Experimental damped response for damper design A. Unbalance, 10.8 g cm.

peak amplitude of lateral vibration was sensed by proximity probes located along the axes designated as X and Y (fig. 3). These proximity probes were located just above the lower ball bearing (fig. 1). Amplitude and phase-angle data were obtained over a speed range from 800 to 10 000 rpm. In most cases, the plots begin at a rotor speed of 2000 rpm. Amplitudes below this speed were too small to plot accurately.

The experimental damping coefficients for each magnet design are presented in table I and were calculated from measured displacement data along each of the two orthogonal axes. These are compared with a theoretical damping coefficient based on the magnet and conductor properties at liquid-nitrogen temperature of −197 °C.

The method used in calculating the damping coefficient from the amplitude-frequency plots is called the one-half power point or quality factor method. This approximation method is accurate for values of dimensionless damping coefficient below 0.1. A description of this method is given in reference 8.

The damped response plots of figure 9 are for a damper assembly consisting of four C-shaped magnets made of cast Alnico 5. The maximum rotor amplitude at the resonant frequency along the X-axis is approximately one-half that along the Y-axis. A damping coefficient of 600 N sec/m was calculated for the X-axis, and a value of 350 N sec/m was calculated for the Y-axis. A theoretical value of 650 N sec/m was calculated for the X-axis and a value of 270 N sec/m was calculated for the Y-axis. The difference in magnitude of damping coefficients in the two orthogonal planes was due to the magnet axes being offset from the proximity-probe axes (X-Y planes) as shown in figure 3.

Design B used the identical, C-shaped Alnico 5 magnets with a low-carbon-steel pole piece added to one pole face. The use of the pole piece decreased the gap width from 0.64 to 0.22 cm, with a corresponding increase in the flux density from 0.54 to 0.7 T, an increase of approximately 30 percent. The rationale for this design was to increase the flux across the gap (B_g in the equation on p. 11).

The damped response for design B is shown in figure 10. Again the peak-to-peak amplitude at resonance along the Y-axis is about twice that along the X-axis. Shown in figure 11 is the orbital motion of the shaft as photographed from the screen of an oscilloscope. The frequency is 6000 rpm, which is close to the resonant frequency. Experimental damping coefficients are 286 N sec/m along the Y-axis and 465 N sec/m along the X-axis. Due to the double peak shown in the amplitude-frequency response along the axis, certain approximations were made regarding the calculation of damping coefficient. Some smoothing of the curve at the resonant peak was necessary in order to obtain a reasonable value of frequency difference ΔN at the one-half power point. The coefficient calculated from magnet and conductor properties was 282 N sec/m. The anticipated increase in damping coefficient for a significant increase in flux density did not occur. Of course, the smaller pole face gap resulted

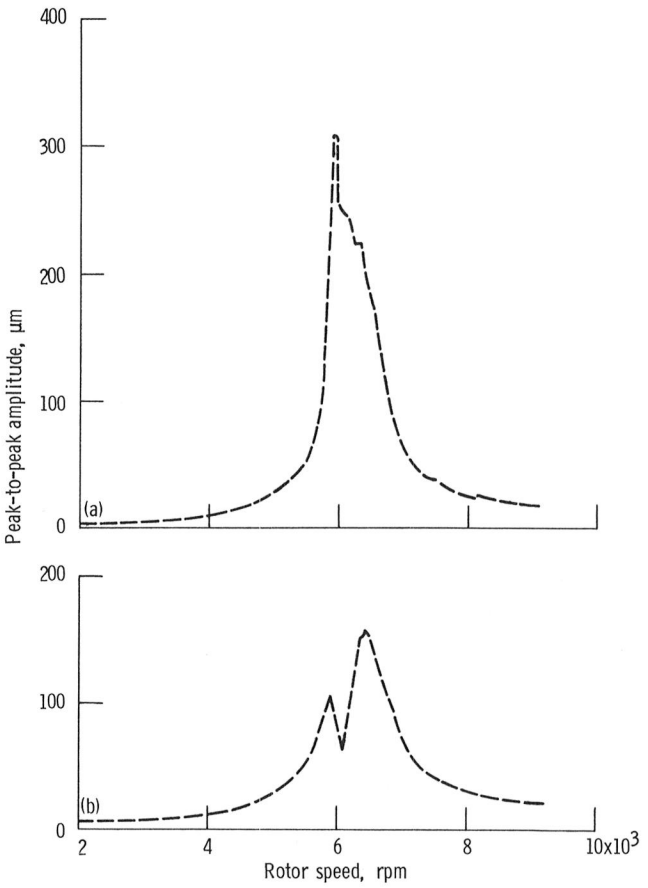

(a) Y-axis. Damping coefficient, C_D, 290 N sec/m.
(b) X-axis. Damping coefficient, C_D, 470 N sec/m.

Figure 10.—Experimental damped response for damper design B. Unbalance, 10.8 g cm.

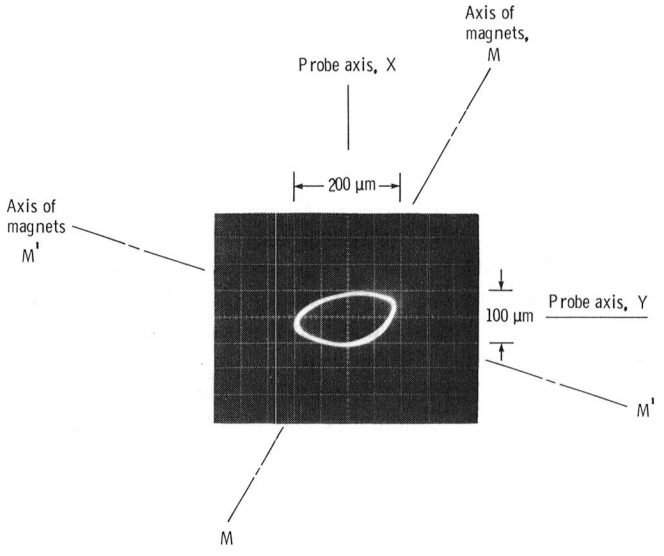

Figure 11.—Damped orbital motion of rotor near resonant frequency of 6000 rpm. Magnet design B; scale factor, V/cm; calibration factor, 78.7 V/cm (200 V/in.).

in the conductors having their volume reduced from 5.1 to 1.7×10^6 m^3, a 66-percent reduction.

Damper design C utilized the high-flux, low-material volume of rare-earth magnet materials, specifically samarium-cobalt (Sm-Co_5). Two pole pieces, with a nominal thickness of 0.64 cm, were attached to the C-shaped Alnico 5 base magnet. Samarium-cobalt magnet material has an energy product (flux density times coercive force at the operating point B_d•H_d) of 144 MJ/m^3 (18 MG Oe). This compares with an energy product of 44.8 MJ/m^3 (5.6 MG Oe) for Alnico 5.

The predicted increase of flux density in the gap did not occur for the combined assembly of the two magnet materials. A calculated value of 0.83 T was predicted from empirical formulas for the combination, but the actual measured value was only 0.59 T. In subsequent discussions the magnet vendor suggested that placing the material with the greater coercive force, (Sm-Co_5) in proximity to the lower coercive-force material (Alnico 5) would result in diminution of flux density in the weaker magnet material.

The plotted response curve for design C (fig. 12) does indicate that this magnet material combination did indeed show greater damping. Coefficients as calculated from the response curve were 430 N sec/m along the *Y*-axis and 570 N sec/m along the *X*-axis. This compared with theoretical values of 780 N sec/m along the *X*-axis and 330 N sec/m along the *Y*-axis. Design C (Sm-Co_5 pole faces) had slightly greater damping than design B (narrow gap) and about the same damping as design A (all Alnico 5).

The amplitude frequency data, as plotted in figure 12, as well as the previous plots are averages, in most cases, of several test runs. A maximum amplitude at the resonant frequency for any one particular test could well have been greater than the average of those plotted. Only test runs of comparative response were averaged in; none of these runs deviated significantly from one another.

Tests were conducted to determine the tare or intrinsic damping of the system. For these tests the magnets were removed from the apparatus. The same magnitude of unbalance was used. The undamped response is plotted as dashed lines in figure 13. Also shown in the same plots are the theoretical responses of this rotor for very light damping. The theoretical data were obtained from an unbalance response code that was modified for circular orbits. Tare damping along the *X*-axis was 70 N sec/m, and the damping along the *Y*-axis was 110 N sec/m. A damping coefficient of 90 N sec/m and a spring stiffness of 2.54×10^6 N/m were used to calculate the theoretical response. The agreement is quite good for the

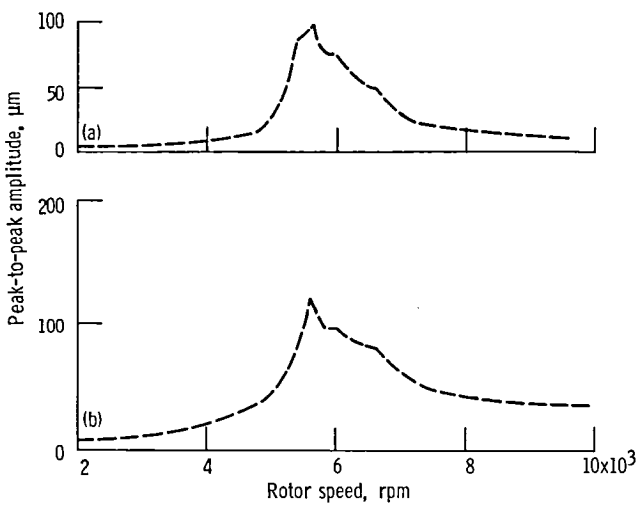

(a) *Y*-axis. Damping coefficient, C_D, 430 N sec/m.
(b) *X*-axis. Damping coefficient, C_D, 576 N sec/m.

Figure 12.—Experimental damped response for damper design C. Unbalance, 10.8 g cm.

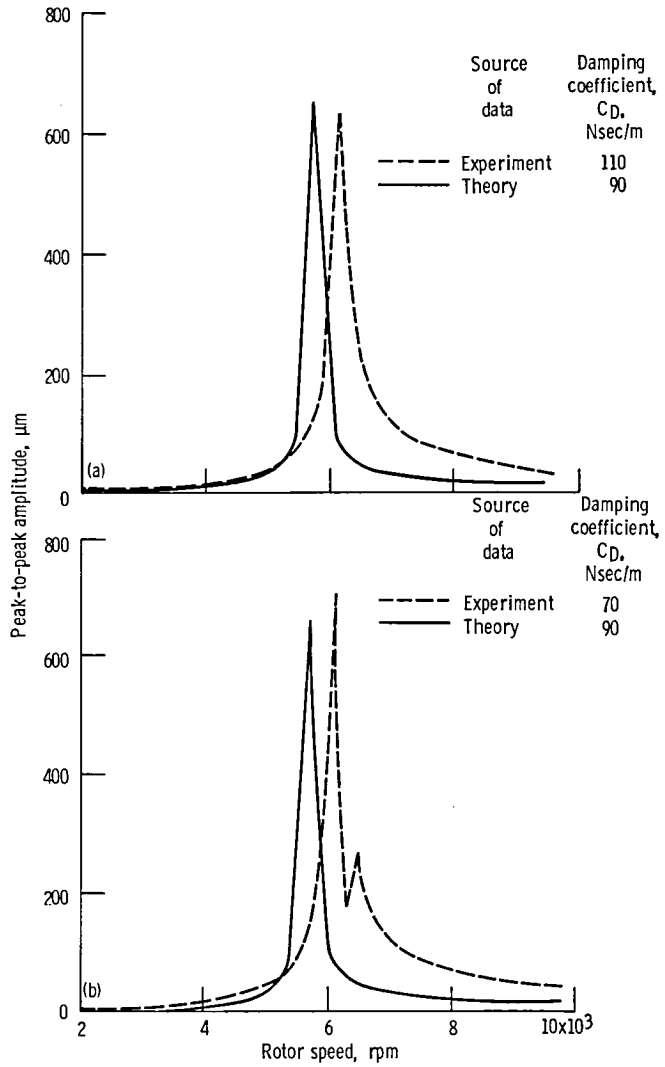

(a) *Y*-axis.
(b) *X*-axis.

Figure 13.—Comparison of theoretical and experimental undamped response. Unbalance, 10.8 g cm; spring stiffness, 2.54 10^6 N/m.

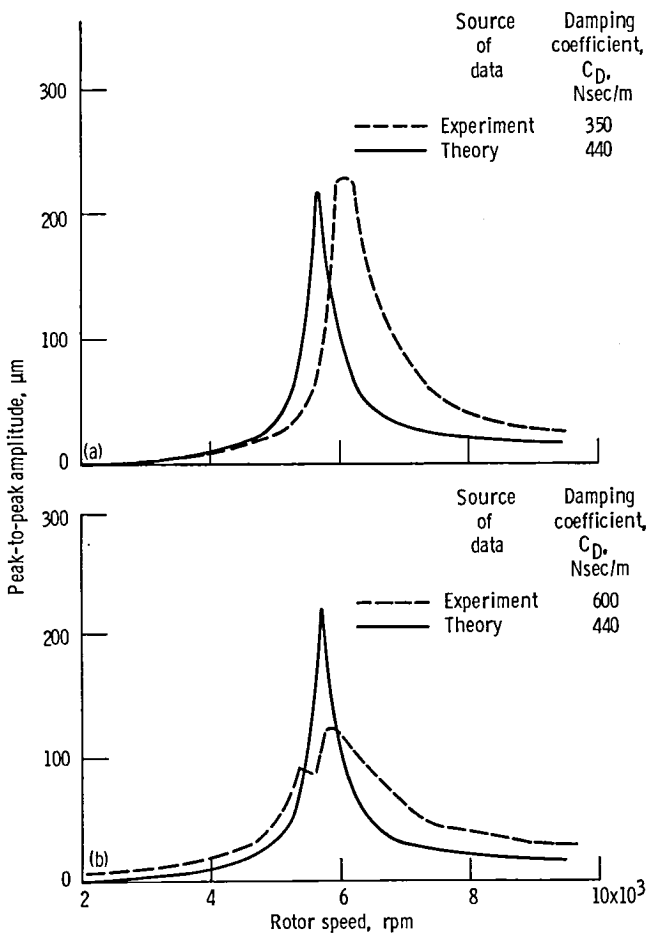

(a) *Y*-axis.
(b) *X*-axis.

Figure 14.—Comparison of theoretical and experimental undamped response. Unbalance, 10.8 g cm; spring stiffness, 2.54 10^6 N/m.

maximum amplitudes and shape; the difference, however, in resonant frequencies is quite large, indicating that the experimental apparatus had a much greater spring rate than that measured statically in room-temperature air. This could account for the discrepancy. A greater spring rate results in a greater resonant frequency.

Figure 14 shows the amplitude-frequency plots for a damped system. For magnet design A an experimental response is shown which is the same as that plotted in figure 9. However, the theoretical damped response (shown as solid lines) has been added to this figure. An unbalance of 10.8 g cm, a spring rate of 2.54×10^6 N/m, and a damping coefficient of 440 N sec/m were the input values in the theoretical response code. This is compared with a measured damping coefficient of 350 N sec/m along the *X*-axis. Since the computer code assumed that the rotor had a circular orbit, rotor response is identical along orthogonal axes. The actual measured amplitude, 120 μm, (the average of two tests) was much less than the theoretical amplitude (210 μm). Agreement is better along the *Y*-axis: 230 μm, actual amplitude; 210 μm, theoretical amplitude from the computer code. The shape of the plot is much broader at the resonant frequency, and suggests much greater damping. The values, however, as calculated by the one-half power-point method, were in fair agreement with the theoretical values.

Summary of Results

A damper assembly that consisted of four equally-spaced, C-shaped, permanent magnets of Alnico 5 magnetic alloy was tested at an unbalance of 10.8 g cm in liquid nitrogen at −197 °C. Damping coefficients of 600 and 350 N sec/m along the orthogonal axes were calculated from measured response data. A theoretical value of 650 N sec/m was calculated for the *X*-axis and of 270 N sec/m for the *Y*-axis by using magnet and conductor properties.

The same C-shaped magnets were modified with a low-carbon-steel pole piece which reduced the gap but increased the flux density. Experimental damping coefficients of 400 and 180 N sec/m were measured and compared with theoretical values of 370 and 150 N sec/m along the *X* and *Y* axes, respectively.

A third magnet design consisted of a C-shaped Alnico 5 magnet with rare-earth samarium-cobalt pole faces. The damping coefficients that were measured along the *X* and *Y* coordinate axes were 500 and 320 N sec/m, respectively. These are compared with the theoretical damping coefficients of 780 and 330 N sec/m along the *X* and *Y* axes, respectively.

With magnets removed from the apparatus, tests were conducted in liquid nitrogen at the same unbalance in order to determine the tare or intrinsic-system damping. Values of 70 and 110 N sec/m were calculated from the measured response along the *X* and *Y* coordinate axes, respectively. At an input value of 90 N sec/m the unbalance-response computer code, which was modified for a circular orbit, compared favorably with the experimental values.

Similarly, a damped theoretical response code was run using a damping coefficient input of 430 N sec/m. The general shape of these plots compares favorably with the experimental plots for a C-shaped magnet of Alnico 5 material. The measured coefficients were 600 and 350 N sec/m along the *X* and *Y* axes, respectively.

Lewis Research Center
National Aeronautics and Space Administration
Cleveland, Ohio, November 22, 1985

References

1. Brown, P.F.: Bearings and Dampers for Advanced Jet Engines. SAE Paper 700318, Apr. 1970.
2. Butner, Miles F.: Dynamic Balance Improvement Program, Final Report, Phase 1. (RI/RD82-285, Rocketdyne; NASA Contract NAS8-34423) NASA CR-170711, 1983, p. 1.
3. Eck, Mathew C.: Solving Subsynchronous Whirl Problems in the High-Pressure Hydrogen Turbomachinery of the SSME. J. Spacecr., vol. 17, no. 3, May-June 1980, pp. 1-9.
4. Crede, Charles E.; and Harris, Cyril M.: Shock and Vibration Handbook, Vol. 2. Data Analysis, Testing, and Methods of Control, McGraw-Hill, 1961, Chapter 32, pp. 32-33.
5. Design and Application of Permanent Magnets. Indiana General, Manual No. 7.
6. Permanent Magnet Design. Thomas Skinner Inc., Bulletin No. M-303, 1969.
7. Schieber, D.: Optimal Dimensions of Rectangular Electromagnets for Breaking Purposes. IEEE Trans. Magn., vol. MAG-11, no. 3, May 1975, pp. 948-952.
8. Crede, Charles E.; and Harris, Cyril M.: Shock and Vibration Handbook, Vol. 1. Basic Theory and Measurements, McGraw-Hill, 1961, pp. 2-15.
9. Hall, L. A.: Survey of Electrical Resistivity Measurements on 16 Pure Metals in the Temperature Range 0 to 273 deg K. NBS-TN-365, National Bureau of Standards, 1968, p. 40.

1. Report No.	2. Government Accession No.	3. Recipient's Catalog No.
NASA TP-2562		

4. Title and Subtitle	5. Report Date
Passive Eddy-Current Damping as a Means of Vibration Control in Cryogenic Turbomachinery	February 1986
	6. Performing Organization Code 506-60-12
7. Author(s) Robert E. Cunningham	8. Performing Organization Report No. E-2762
	10. Work Unit No.
9. Performing Organization Name and Address National Aeronautics and Space Administration Lewis Research Center Cleveland, Ohio 44135	11. Contract or Grant No.
	13. Type of Report and Period Covered Technical Paper
12. Sponsoring Agency Name and Address National Aeronautics and Space Administration Washington, D.C. 20546	14. Sponsoring Agency Code

15. Supplementary Notes

16. Abstract

Lateral shaft vibrations produced by a rotating unbalance weight were damped by means of eddy currents generated in copper conductors that were precessing cyclicly in the gap formed by the pole faces of C-shaped, permanent magnets. The damper assembly, which was located at the lower bearing support of a vertically oriented rotor, was completely immersed in liquid nitrogen during the test run. The test rotor was operated over a speed range from 800 to 10 000 rpm. Three magnet/conductor designs were evaluated. Experimental damping coefficients varied from 180 to 530 N sec/m. Reasonable agreement was noted for theoretical values of damping for these same assemblies. Values of damping coefficients varied from 150 to 780 N sec/m. The results demonstrate that passive eddy-current damping is a viable candidate for vibration control in cryogenic turbomachinery.

17. Key Words (Suggested by Author(s))	18. Distribution Statement
Eddy currents; Damping; Rotor dynamics; Bearings; Magnetics; Cryogenics; Turbopumps	Unclassified - unlimited STAR Category 15

19. Security Classif. (of this report)	20. Security Classif. (of this page)	21. No. of pages	22. Price*
Unclassified	Unclassified	12	A02

*For sale by the National Technical Information Service, Springfield, Virginia 22161

NASA-Langley, 1986

National Aeronautics and
Space Administration
Code NIT-4

Washington, D.C.
20546-0001